Lithiophilic 3D-Si/SiO_x host for dendrite free Lithium Metal Battery via simple Magnesiothermic Reduction process

Asif Raza,[a] Jae-Yeon Bang,[c] Hyo-yeong Kim,[c] Jeong-Hee Choi,[a,b] Hae-Young Choi,[b] Sang-Min Lee,[c,d]*

[a] Electro–Functionality Material Engineering, University of Science and Technology (UST), Daejeon, 34113, Republic of Korea

[b] Battery Research Division, Korea Electrotechnology Research Institute, Changwon, 51543, Republic of Korea

[c] Department of Battery Engineering, Graduate Institute of Ferrous & Energy Materials Technology (GIFT), Pohang University of Science and Technology, Pohang, 37673, Republic of Korea

[d] Department of Materials Science & Engineering, Pohang University of Science and Technology, Pohang, 37673 Republic of Korea

Corresponding Authors

* E–mail: sangma@postech.ac.kr(Sang-Min Lee)

Lithiophilic 3D-Si/SiO_x host for dendrite free Lithium Metal Battery via simple Magnesiothermic Reduction process

Abstract

In the development of renewable energy sources, batteries are considered the best option for energy storage. High energy density and high performance are key demands for emerging technologies. Lithium-metal batteries (LMBs) are considered promising candidates for storing generated energy. However, the formation of lithium dendrites and infinite volume expansion during cycling are serious limitations in current LMB applications. 3D-structured anodes have received considerable attention as an effective solution to overcome these problems. Herein, we synthesize a lithiophilic 3D-Si/SiO_x host for LMBs via a simple magnesiothermic reduction process (MRP). The 3D porous SiO_x structure provides a large specific surface area, which reduces local current density and offers ample space for Li deposition. The 3D-Si/SiO_x anode not only accommodates volume changes but also demonstrates homogeneous, dendrite-free lithium deposition with a high coulombic efficiency of more than 99% at 0.1, 0.5, and 1.0C. The symmetric cell composed of prelithiated (4 mAh/cm^2) 3D-Si/SiO_x shows stable long-cycle performance for over 350 hours. By utilizing a single porous particle material with surface-limited lithiophilic properties, rather than the conventional complex 3D lithium anode designs (which typically involve hierarchical structures and lithium-friendly seed materials), this work provides new insights into the design of 3D lithium metal anodes.

Keywords: Lithiophilic 3D host, Si-based anode, Lithium-metal batteries

Impact Statements: This research demonstrates the potential application of silicon oxide as an anode material for lithium metal batteries, while also providing guidelines for the design of porous structures at the particle level.

1. Introduction

Demands are increasing for high-energy storage devices as a power source for emerging technologies, such as electric vehicles and energy storage systems. Lithium-ion battery (LIB) was recognized as an inimitable and exceptional power source since its commercialization [1,2]. However, the energy density of LIBs has increased to its limitation (250 W h kg^{-1}) over the past few decades and extensive research has been done for an alternative next-generation battery [3,4]. Lithium metal as an anode is a possible candidate rather than graphite owing to its 10-fold higher theoretical capacity and low electrochemical potential (−3.04 V vs H_2/H^+), which makes lithium metal anode a dominant candidate [5–7]. As a result, Li metal has become a competitive choice for next-generation energy storage systems and has been applied in Li metal batteries (LMBs) [8]. However, the instability of solid electrolyte interphases (SEI) and volume changes during the plating/stripping cause low coulombic efficiency (CE), and safety issues like dendrite growth are serious problems in the commercialization of LMB [9–11].

To overcome the above issues in LMB, numerous strategies have been investigated, such as electrolyte modification by additives to create an artificial SEI layer, dendrite inhibiting protecting layer, separator modification, and three dimensional (3D) structured anode as lithium host [12–19]. 3D structured anodes are the most accepted efficient strategy in LMB to increase the specific surface area as ample space for metallic Li accommodation also decreases the local current density [3,6,9,20]. Based on this design concept, several 3D anodes have been introduced such as Carbon, Cu, Au, Ni, and their foam structures [21–25]. These metallic 3D hosts demonstrated an outstanding cycling performance by homogenous plating/striping behaviors of Li. However, the high density of the metallic host leads to a significant reduction in the energy density of LMB [19]. On other hand carbon-based 3D hosts have gained much attraction with low mass density, stable electrochemistry, and high electrical conductivity [9]. However, the lithiophobic nature of carbon makes it difficult for Li to depose into the hollow cavity of carbon [26]. Thus, the extra treatment required to make is lithiophilic, which may cause extra costs in the fabrication of suitable Li-host.

Silicon suboxides have been widely investigated as substitute anode materials for lithium-ion batteries (LIB) [27,28]. Additionally, the electrochemical reduction of SiO_x to Li_xSi and Li_2O makes it quite a lithiophilic anode. Hence, the potential of SiO_x for the designing of high-

performance Li metal anodes has also been discovered. *In-situ* generated Li_xSi-Li_2O matrix can be functionalized as nano-seeds to regulate the homogeneous nucleation and dendrite-free deposition of Li-Metal [29].

Herein, we synthesized the super-lithiophilic 3D-Si/SiO_x host for lithium metal battery via a simple magnesiothermic reduction process. The magnesiothermic reduction process (MRP) is a straightforward and effective cost technique for transforming various silica sources into porous silicon. This process operates at a relatively low temperature due to the low melting point of magnesium, making the process both practical and economical [27,30,31]. The unique structure provides sufficient space to well control the volume expansion during the lithium plating/stripping along with the inhibition of dendrite growth. The presence of the reduced crystalline Si (c-Si) phase and its porous structure provides space to accommodate the stored lithium while imparting lithiating properties to the electrode. The newly designed 3D-Si/SiO_x electrode demonstrates better cyclic performance when compared with that of pristine SiO_x and produces better coulombic efficiency of more than 99%. Additionally, the 3D-Si/SiO_x anode maintained a long cycle life for more than 700h after continuous plating/striping during the symmetric cell test for 2 mAh cm^{-2} @ 2 mA cm^{-2}. This study offers novel insights that can be utilized to achieve consistent lithium deposition, addressing challenges related to dendrite formation within a three-dimensional structure. These findings have the potential to advance the development of high-performance lithium metal anodes.

2. Experimental Section

2.1 Material Synthesis:

3D-Si/SiO_x was prepared by a simple magnesiothermic reaction. Typically SiO (Silicon (II) oxide, 99.8%, Alfa Aesar), and Mg (Magnesium metal powder, Fisher Scientific U.K.) were mixed in a weight ratio of 1:0.5 by hand in a motor and transferred to a glass tube furnace in a ceramic crucible covered with a cap and heated at 700 °C for 2 h under inert environment. Later on, when the furnace cooled to room temperature, the powder was collected and washed with 2M HCl solution to remove the MgO and byproducts followed by DI washing and vacuum drying at 100 °C for 12

hours. Mg_2SiO_4@p-SiO_x and p-SiO_x (porous SiO_x) were synthesized by mixing SiO_x with KCl and Mg, followed by the heat treatment at distinct temperatures: 750°C for p-SiO_x and 800°C for Mg_2SiO_4@p-SiO_x.

2.2 Material Characterization:

X-ray diffraction (XRD) patterns were recorded using a Rigaku instrument under Cu Kα radiation (λ = 1.5406 Å). Scanning Electron Microscopy (FE-SEM) and X-ray spectrometer (EDS) were conducted on a Field emission scanning electron microscope (Hitachi S-4800). Transmission electron microscopy (TEM) and high-resolution-TEM (HRTEM) images were taken using a field emission transmission electron microscope (FE-TEM) (FEI Titan G2 Themis STEM CS Probe). The specific surface areas, pore sizes, and pore volumes were calculated by Brunauer−Emmett−Teller (BET) method using Quantachrome. ThermoFisher (NEXSA, Al Kα, 1486.6 eV) was used to record X-ray photoelectron spectroscopy (XPS) spectra.

2.3 Electrochemical Testing:

All electrochemical testing was done using the 2032 coin-type cell assembled in an argon-filled glovebox with H_2O and O_2 levels below 0.1ppm using 500 μm thick lithium metal foil as counter electrode and Celgard 3501 separator of 25 μm thickness. The electrodes were fabricated using the casting method of slurry on Cu foil. The slurry mixture of Li host material, super P, carboxymethyl cellulose (CMC), and poly (acrylic acid) (PAA) in a weight ratio of 80:5:7.5:7.5, respectively, in deionized water spread on Cu foil using a doctor blade. The electrolyte used was composed of 1 M Bis(trifluoromethane)sulfonamide Lithium salt (LiTFSI) in 1,3-Dioxolane (DOL) and 1,2-Dimethoxyethane (1:1, v/v) with 10 wt% of Lithium nitrate, 99.999% ($LiNO_3$) additive. The half-cells were Galvanostatically discharged/charged at 0.1C, 0.5C, and 1.0C after the 3 pre-cycles at 0.1C and 4 mAh cm^{-2} Li was plated at the first cycle.

For symmetric cells, to obtain the Li metal working electrode (Li@3D-Si/SiO_x), 4 mAh cm^{-2} of Li was pre-deposited onto 3D-Si/SiO_x anode at 0.1C and tested at different current densities with Li-deposition capacity of 1 mAh cm^{-2}.

3. Result and Discussion

3D-Si/SiO_x was synthesized via a simple magnesiothermic reduction process shown in Fig. 1a. 1.0g of SiO and 0.5g of Mg were mixed and heated at 700 °C for 2 h in a glass tube furnace in an inert environment followed by 2M HCl and DI washing and drying for 12 h in a vacuum oven at 100 °C. Fig. 1(b and c) show the SEM images before and after the magnesiothermic reaction, respectively. Pristine SiO (Figure 1b) has a very smooth surface while 3D-Si/SiO_x (Figure 1c, Figure S1) shows a very rough surface like lava rock after the reduction and acid treatment. The 3D surface morphology was created by Mg etching oxygen from SiO to form MgO. The MgO was later removed by HCl treatment. [31].

Figure 1

The crystalline structure of pristine SiO and synthesized 3D-Si/SiO_x powder is characterized by X-ray diffraction (XRD) analysis and shown in figure 2a. The XRD pattern of 3D-Si/SiO_x shows well-indexed diffraction peaks at 28.4, 47.3, 56.1, 69.1, and 76.3°, which corresponds to the crystalline planes of {111}, {220}, {311}, {331}, and {422}, respectively (JCPDS 27-1402), whereas the XRD pattern of pristine SiO shows a broad peak at Bragg angle (2θ) of 21.5° indicating the amorphous nature. Moreover, the additional reflections of Mg_2SiO_4 byproduct formed during the reduction process are also observed in diffraction pattern of 3D-Si/SiO_x, which cannot be removed by HCl treatment [27]. At the outer surface of SiO particles, $MgSiO_3$ and Si formation were initiated by a gas−solid reaction between Mg and SiO then, Mg_2SiO_4 as an intermediate phase is formed before the reaction (MgO formation) reaching thermodynamic equilibrium [32]. Cross-sectional TEM-EDX image was analyzed to further confirm the 3D structure and Mg_2SiO_4 doping in 3D-Si/SiO_x as shown in Figure S2. It is shown that surface have enough large pores greater than 1μm to create 3D structure and Mg_2SiO_4 is well distribute in the particle. The surface composition of SiO and 3D-SiOx was analyzed by XPS shown in Figure S3a and S3b, respectively. The Deconvoluted Si 2P spectrum (Figure 2b) shows each oxidation state of Si to determine the metallic Si. It is confirmed the high areal amount of metallic Si improves the conductivity and lithiophilic properties of the material as compared to pristine SiO (Figure S3c).

Figure 2c shows Mg1s spectra, which also confirm the formation of Mg_2SiO_4 in the 3D-Si/SiO_x, which corresponds well to XRD analysis. Mg_2SiO_4 is expected to be a predominant electronic

conductor that can effectively sustain the volume expansion of the composites during cycles and is assumed to have a lithiophilic property [27,32,33].

Figure 2

In addition, SiO and 3D-Si/SiO_x anodes were further characterized by BET analysis presented in figure 2d. Both samples show the H3 hysteresis loop of type IV isotherm indicating the slit-shaped porous structure. The BET specific surface area of 3D-Si/SiO_x (42.35 m^2 g^{-1}) is much larger than pristine SiO (1.273 m^2 g^{-1}) with a total pore volume of 0.078, and 0.0065 cm^3 g^{-1} (Table 1, Figure S4), respectively. During the magnesiothermic reaction, the formation of MgO and etching by acid treatment cause the formation of a 3D structure at the surface of SiO which attribute to the high surface area and large pore volume. The BET analysis is summarized in the Table. 1

Table 1

4. Electrochemical Analysis

To evaluate the lithium plating/stripping behavior on the surface of prepared electrodes, the first 8 mAh cm^{-2} of lithium was platted on pristine, and 3D-Si/SiO_x are shown in Figure 3. 3D-Si/SiO_x electrode (Figure 3a) shows the flat and smooth surface confirms the homogenous plating of lithium without any evidence of Li dendrite. In contrast, pristine SiO (Figure 3c) shows a rough surface with uneven lithium plating and obviously, Li dendrite can be observed. Furthermore, when half of the plated lithium was striped (4 mAh cm^{-2}), 3D-Si/SiO_x (Figure 3b) shows the remaining lithium is well intact on the surface due to the 3D porous structure and lithiophilic property of the 3D-Si/SiO_x. The presence of Mg in the composite is also believed to help protect the lithium within the 3D-Si/SiO_x from further removal. [34]. Whereas pristine SiO shows no lithium, all the lithium has washed out due to the non-lithiophilic and flat surfaces of pristine SiO. The lithiophilic property of 3D-Si/SiO_x was also confirmed with cross-section SEM images of Li-plated electrodes shown in Figure S5. Figure S5a, 3D-Si/SiO_x shows the good contact between plated lithium and electrode without any gap. Whereas Figure S5b of pristine SiO shows a large gap between plated lithium and the electrode. This demonstrates the Mg_2SiO_4 doped in 3D-Si/SiO_x induces lithiophilic property and uniform deposition of lithium and also inhibits the Li dendrite formation. To further understand the role and lithiophilic properties of Mg_2SiO_4, we conducted

additional mechanistic studies(Figure S6). We synthesized two sets of porous SiO_x, one doped with Mg_2SiO_4 and one without, determined by the heat treatment temperature. During the lithium plating tests, the Mg_2SiO_4-doped porous SiO_x(-24mV) exhibited lower overpotentials. This result indicates that Mg_2SiO_4 enhances lithiophilic properties, reducing overpotentials during plating.

Figure 3

The electrochemical performance was evaluated for Pristine SiO and prepared 3D-Si/SiO_x are shown in Figure 4. Figure 4a shows the voltage profile of Li plating at the first cycle. Both samples show a smooth voltage curve without any voltage drop. 3D-Si/SiO_x exhibited the larger plateau region indicating the conversion reaction which is favorable in the smooth lithium plating/stripping as compared to the pristine SiO. *In-situ* generated Li_xSi-Li_2O matrix can be functionalized as nano-seeds to regulate the homogeneous nucleation and dendrite-free deposition of Li-metal [29]. The cyclic performance of the electrodes was evaluated by coulombic efficiency in a half-cell constructed using Li-foil as a counter electrode. At the first cycle, 4 mAh cm^{-2} of lithium was plated and striped at 0.1C. until the cut-off voltage of 1.0 V. Following this, 1 mAh cm^{-2} of lithium was plated and stripped to determine the cycling performance at 0.1C and 0.5C are shown in figure 4b and 4c, respectively. As shown, the coulombic efficiency of pristine SiO initially improved in a few cycles and then dramatically degrade, and even cell short happened before the 80 cycles, however, the 3D-Si/SiO_x anode shows the CE reached more than 99% after a few cycles and maintained it for 100 cycles without any fluctuation. Even at a higher C-rate of 1.0 C, the 3D-Si/SiO_x anode shows remarkable performance and maintained an average CE of ~99.% as shown in Figure S6. The average CE of 3D-Si/SiO_x and pristine SiO at various C-rate is shown in Figure 4d. Comparative studies of the different 3D- lithium host are listed in a Table. S1. Furthermore, the contribution of crystalline silicon phase in 3D host was analyzed by limiting lithium-striping to 0.2 V of cutoff voltage as shown in Figure S7. Figure S7a shows 4 mAh cm^{-2} of lithium was plated on 3D-Si/SiO_x host. The initial capacity until 0.5 mAh cm^{-2} and then 2.65 mAh cm^{-2} arise from the electrochemical contribution of additive carbon black and metallic Si, respectively. To restrict this, we stripped the lithium until the cut-off voltage 0.2V (Figure S7b) and further cycles were carried out at 1 mAh cm^{-2} @1C. The 3D-Si/SiO_x still exhibited the average coulombic efficiency of 95% at 0.5 and 1.0C shown in Figure S7c.

Figure 4

Cross-section SEM analyses were conducted to determine the change in 3D-Si/SiO_x electrode thickness after 4 and 8 mAh cm^{-2} of lithium plating. When 4 and 8 mAh cm^{-2} of lithium was plated, 3D-Si/SiO_x electrode thickness was measured as 60 and 72 μm corresponding to 29.9 and 55.9% (Figure 5a and 5b), respectively as compared to the fresh electrode. 3D-Si/SiO_x electrode thickness at after 100^{th} cycle was measured as 77.2 μm (Figure 5d) which is corresponding to only 28.7%, compared with 4 mAh cm^{-2} lithium-plated electrode. It is confirmed that the 3D structure effectively accommodates the stress induced by volume changes during lithium plating.

Figure 5

To determine the impedance changes and cell failure by dendrite, the voltage hysteresis and cycle stability of the electrode were evaluated by a constant current charge-discharge cycle experiment as shown in Figure 6. Firstly, 4 mAh cm^{-2} of lithium was deposited into a pristine SiO and 3D-Si/SiO_x electrode by electrochemical lithiation and sandwitched with another electrode with the same areal capacity [Li-SiO/Li-SiO, Li-3D-Si/SiO_x /Li-3D-Si/SiO_x]. The symmetric cell test was conducted at a constant current density of 1 mA cm^{-2}, with a cutoff areal capacity of 1 mAh cm^{-2}, corresponding to 25% of the Li utilization ratio based on pre-deposited lithium amount. Pre-lithiated 3D-Si/SiO_x symmetry cell shows excellent cycling stability until 375 h with a stable overpotential of ~40mV, whereas the overpotential of prelithiated SiO symmetry cell suddenly increased earlier than 3D-Si/SiO_x anode only after 300 h, which may be caused by the Li dendrite and dead-Li formation. Additionally, when the areal capacity and current density were increased to 2 mAh cm^{-2} and 2 mA cm^{-2}, the prelithiated 3D-Si/SiO_x symmetry cell showed the consistent overpotential (160 mV) up to 700 h whereas the prelithiated SiO symmetry cell does not produce sufficient data (Figure 6b).

Figure 6

To reveal the significance of 3D-Si/SiO_x host material, a coin type full-cell test was carried out. The 3D-Si/SiO_x electrode was pre-lithiated to be 4 mAh cm^{-2} by electrochemical lithiation process and paired with LFP cathode with corresponding areal capacity based on N/P=1.1. The electrochemical performance of the 3D-Si/SiO_x-LFP cell was compared with that of a cell containing 20 μm thick 2D-Li foil, corresponding to 4 mAh cm^{-2}. The charge and discharge

currents applied to the full cell were based on the weight of LFP and were activated at 0.1C (1C = 170 mAh g^{-1}) for the first cycle of formation stage and at 0.5C for the subsequent cycles. Figure 7a shows that the initial discharge capacities of LFP/3D-Si/SiO_x and LFP/Li(20 μm) are 160.6 and 154.5 mAh g^{-1} at 0.1 C, respectively. As illustrated in Figure 7b, 3D-Si/SiO_x demonstrated a better cyclic performance with no significant capacity loss even after 70 cycles and maintained an average CE of ≈99%, indicating the stable reversibility of 3D-Si/SiO_x during the repeated Li plating/stripping. In comparison, LFP/Li(20μm) cell demonstrated lower cycle stability and its capacity decreased abruptly and the cell does not produce further data after just 30 cycles. This could be attributed to the formation of Li irregular depositions and Li-dendrite during the long-term Li plating/stripping. To demonstrate the practical applicability of 3D-SiO_x, we conducted a rate performance test (Figure S9). Compared to Li metal, 3D-SiO_x exhibited a high-capacity retention at high rates, indicating that this material performs exceptionally well in fast-charging environments.

Figure 7

5. Conclusion

In summary, the 3D-Si/SiO_x anode was developed through a magnesiothermic reduction process using micro-size SiO with Mg_2SiO_4 doping as a lithiophilic host for LMB. The 3D structure with a large surface area provides sufficient space to accommodate lithium plating, which also avoids volume changes caused by high levels of lithiation reaction. In addition, dead lithium formation by lithium dendritic growth mechanism was effectively suppressed by the highly lithiophilic 3D-Si/SiO_x frame during lithium stripping/plating process. Unlike previous studies that proposed complex design strategies to deposit lithium-affinity materials onto an inactive frame and implement a hierarchical three-dimensional structure for a three-dimensional lithium anode, this study provides novel data that can be applied to achieve uniform lithium deposition while overcoming the lithium dendrite growth problem by easily implementing a 3D Si/SiO_x structure that has lithiophilic property on the surface and the frame material itself can store lithium through a simple one-time process, thereby contributing to the development of high-performance lithium metal anodes with suppressed volume change.

Supplementary Materials

Supplementary data for this article can be found in the online version at XXX

Author Contributions

Asif Raza and J.Y.B. contributed equally to this work. The manuscript was written through contributions of all authors. All authors have given approval to the final version of the manuscript.

Disclosure statement

The authors declare no competing financial interest.

Acknowledgements

This research was supported by the 'Regional Innovation Mega Project' program through the Korea Innovation Foundation, funded by the Ministry of Science and ICT (Project Number: 2023-DD-UP-0332); The Technology Development Program (2022M3J1A1055349) funded by the Ministry of Science, ICT & Future Planning; and the Korea Institute for Advancement of Technology (KIAT) grant, funded by the Korean Government (MOTIE) (P00419413, HRD Program for Industrial Innovation).

References:

[1] Dunn B, Kamath H, Tarascon JM. Electrical Energy Storage for the Grid: A Battery of Choices. Science. 2011 Nov 18;334(6058):928-935. DOI:10.1126/science.1212741

[2] Mai LQ, Yan MY, Zhao YL. Track batteries degrading in real time. Nature. 2017 Jun 22;546(7659):469-470. DOI 10.1038/546469a

[3] Zhang X, Yang YA, Zhou Z. Towards practical lithium-metal anodes. Chem Soc Rev. 2020 May 21;49(10):3040-3071. DOI: 10.1039/c9cs00838a

[4] Li S, Jiang MW, Xie Y, et al. Developing High-Performance Lithium Metal Anode in Liquid Electrolytes: Challenges and Progress. Adv Mater. 2018 Apr 25;30(17). DOI: 10.1002/adma.201706375

[5] Yan C, Cheng XB, Yao YX, et al. An Armored Mixed Conductor Interphase on a Dendrite-Free Lithium-Metal Anode. Adv Mater. 2018 Nov;30(45). DOI:10.1002/adma.201804461

[6] Cheng XB, Zhang R, Zhao CZ, Zhang Q. Toward Safe Lithium Metal Anode in Rechargeable Batteries: A Review. Chem Rev. 2017 Aug 9;117(15):10403-10473. DOI: 10.1021/acs.chemrev.7b00115

[7] Xu W, Wang JL, Ding F, et al. Lithium metal anodes for rechargeable batteries. Energ Environ Sci. 2014 Feb;7(2):513-537. DOI: 10.1039/c3ee40795k

[8] Lin DC, Liu YY, Cui Y. Reviving the lithium metal anode for high-energy batteries. Nat Nanotechnol. 2017 Mar;12(3):194-206. DOI: 10.1038/Nnano.2017.16

[9] Ye H, Xin S, Yin YX, Guo YG. Advanced Porous Carbon Materials for High-Efficient Lithium Metal Anodes. Adv Energy Mater. 2017 Dec 6;7(23). DOI:10.1002/aenm.201700530

[10] Cohen YS, Cohen Y, Aurbach D. Micromorphological studies of lithium electrodes in alkyl carbonate solutions using in situ atomic force microscopy. J Phys Chem B. 2000 Dec 28;104(51):12282-12291. DOI: 10.1021/jp002526b

[11] Wood KN, Kazyak E, Chadwick AF, et al. Dendrites and Pits: Untangling the Complex Behavior of Lithium Metal Anodes through Operando Video Microscopy. Acs Central Sci. 2016 Nov 23;2(11):790-801. DOI: 10.1021/acscentsci.6b00260

[12] Wang XF, Zhang MH, Alvarado J, et al. New Insights on the Structure of Electrochemically Deposited Lithium Metal and Its Solid Electrolyte Interphases via Cryogenic TEM. Nano Lett. 2017 Dec;17(12):7606-7612. DOI:10.1021/acs.nanolett.7b03606

[13] Zhang D, Wang S, Li B, et al. Horizontal Growth of Lithium on Parallelly Aligned MXene Layers towards Dendrite-Free Metallic Lithium Anodes. Adv Mater. 2019 Aug;31(33). DOI: 10.1002/adma.201901820

[14] Li YJ, Wang WY, Liu XX, et al. Engineering stable electrode-separator interfaces with ultrathin conductive polymer layer for high-energy-density Li-S batteries. Energy Storage Mater. 2019 Dec;23:261-268. DOI: 10.1016/j.ensm.2019.05.005

[15] Zhang WD, Wu Q, Huang JX, et al. Colossal Granular Lithium Deposits Enabled by the Grain-Coarsening Effect for High-Efficiency Lithium Metal Full Batteries. Adv Mater. 2020 Jun;32(24). DOI: 10.1002/adma.202001740

[16] Wu X, Liu NN, Guo ZK, et al. Constructing multi-functional Janus separator toward highly stable lithium batteries. Energy Storage Mater. 2020 Jun;28:153-159. DOI: 10.1016/j.ensm.2020.03.004

[17] Ye WB, Pei F, Lan XN, et al. Stable Nano-Encapsulation of Lithium Through Seed-Free Selective Deposition for High-Performance Li Battery Anodes. Adv Energy Mater. 2020

Feb;10(7). DOI: 10.1002/aenm.201902956

[18] Yu C, Du Y, He RH, et al. Hollow SiO_x/C Microspheres with Semigraphitic Carbon Coating as the "Lithium Host" for Dendrite-Free Lithium Metal Anodes. Acs Appl Energ Mater. 2021 Apr 26;4(4):3905-3912. DOI: 10.1021/acsaem.1c00290

[19] Noh HJ, Lee MH, Kim BG, et al. 3D Carbon-Based Porous Anode with a Pore-Size Gradient for High-Performance Lithium Metal Batteries. Acs Appl Mater Inter. 2021 Nov 24;13(46):55227-55234. DOI: 10.1021/acsami.1c17616

[20] Zhang R, Li NW, Cheng XB, et al. Advanced Micro/Nanostructures for Lithium Metal Anodes. Adv Sci. 2017 Mar;4(3). DOI: 10.1002/advs.201600445

[21] Yan K, Lu ZD, Lee HW, et al. Selective deposition and stable encapsulation of lithium through heterogeneous seeded growth. Nat Energy. 2016 Feb 22;1. DOI:10.1038/Nenergy.2016.10

[22] Yun QB, He YB, Lv W, et al. Chemical Dealloying Derived 3D Porous Current Collector for Li Metal Anodes. Adv Mater. 2016 Aug 24;28(32):6932. DOI: 10.1002/adma.201601409

[23] Xu YL, Menon AS, Harks PPRML, et al. Honeycomb-like porous 3D nickel electrodeposition for stable Li and Na metal anodes. Energy Storage Mater. 2018 May;12:69-78. DOI: 10.1016/j.ensm.2017.11.011

[24] Fang YJ, Zeng YX, Jin Q, et al. Nitrogen-Doped Amorphous Zn-Carbon Multichannel Fibers for Stable Lithium Metal Anodes. Angew Chem Int Edit. 2021 Apr 6;60(15):8515-8520. DOI: 10.1002/anie.202100471

[25] Fang YJ, Zhang SL, Wu ZP, et al. A highly stable lithium metal anode enabled by Ag nanoparticle-embedded nitrogen-doped carbon macroporous fibers. Sci Adv. 2021 May;7(21). DOI: ARTN eabg362610.1126/sciadv.abg3626

[26] Lin DC, Liu YY, Liang Z, et al. Layered reduced graphene oxide with nanoscale interlayer gaps as a stable host for lithium metal anodes. Nat Nanotechnol. 2016 Jul;11(7):626. DOI: 10.1038/Nnano.2016.32

[27] Raza A, Jung JY, Lee CH, et al. Swelling-Controlled Double-Layered $SiO_x/Mg_2SiO_4/SiO_x$ Composite with Enhanced Initial Coulombic Efficiency for Lithium-Ion Battery. Acs Appl Mater Inter. 2021 Feb 17;13(6):7161-7170. DOI: 10.1021/acsami.0c19975

[28] Liu ZH, Yu Q, Zhao YL, et al. Silicon oxides: a promising family of anode materials for lithium-ion batteries. Chem Soc Rev. 2019 Jan 7;48(1):285-309. DOI: 10.1039/c8cs00441b

[29] Wang HS, Cao X, Gu HK, et al. Improving Lithium Metal Composite Anodes with Seeding and Pillaring Effects of Silicon Nanoparticles. Acs Nano. 2020 Apr 28;14(4):4601-4608. DOI: 10.1021/acsnano.0c00184

[30] Wang BR, Li WW, Wu T, et al. Self-template construction of mesoporous silicon submicrocube anode for advanced lithium ion batteries. Energy Storage Mater. 2018 Nov;15:139-147. DOI: 10.1016/j.ensm.2018.03.025

[31] Raza A, Kim SY, Choi JH, et al. Crystallinity-controlled SiO_x anode material prepared through a salt-assisted magnesiothermic reduction for lithium-ion batteries. Int J Energ Res. 2022 Oct 25;46(13):18269-18277. DOI: 10.1002/er.8443

[32] Zhang Y, Guo GN, Chen C, et al. An affordable manufacturing method to boost the initial Coulombic efficiency of disproportionated SiO lithium-ion battery anodes. J Power Sources. 2019 Jun 30;426:116-123. DOI:10.1016/j.jpowsour.2019.04.032
[33] Sun WQ, Dai LD, Hu HY, et al. Experimental Research on Electrical Conductivity of the Olivine-Ilmenite System at High Temperatures and High Pressures. Front Earth Sc-Switz. 2022 Apr 5;10. DOI: 10.3389/feart.2022.861003
[34] Wu C, Huang HF, Lu WY, et al. Mg Doped Li-LiB Alloy with In Situ Formed Lithiophilic LiB Skeleton for Lithium Metal Batteries. Adv Sci. 2020 Mar;7(6). DOI:10.1002/advs.201902643

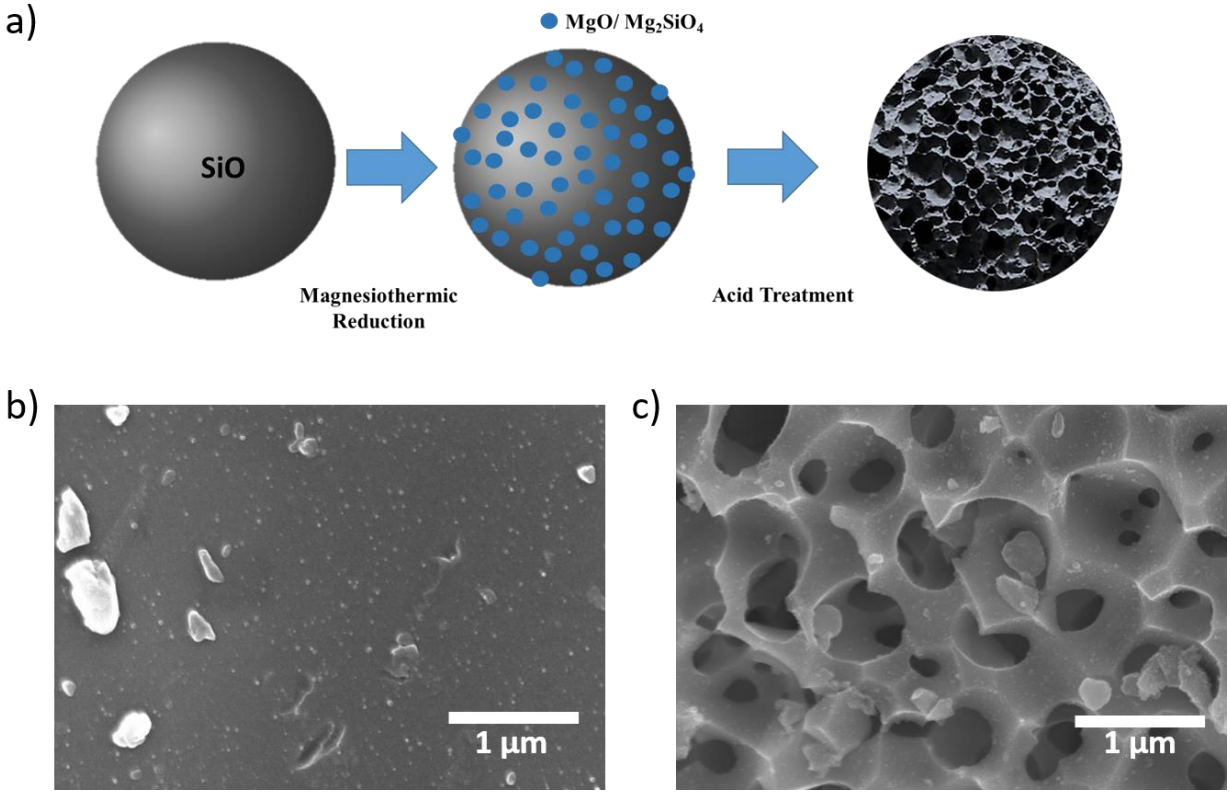

Figure 1: (a) Synthesis scheme for 3D-SiO. SEM image of (b) Pristine SiO and, (c) 3D-Si/SiO_x.

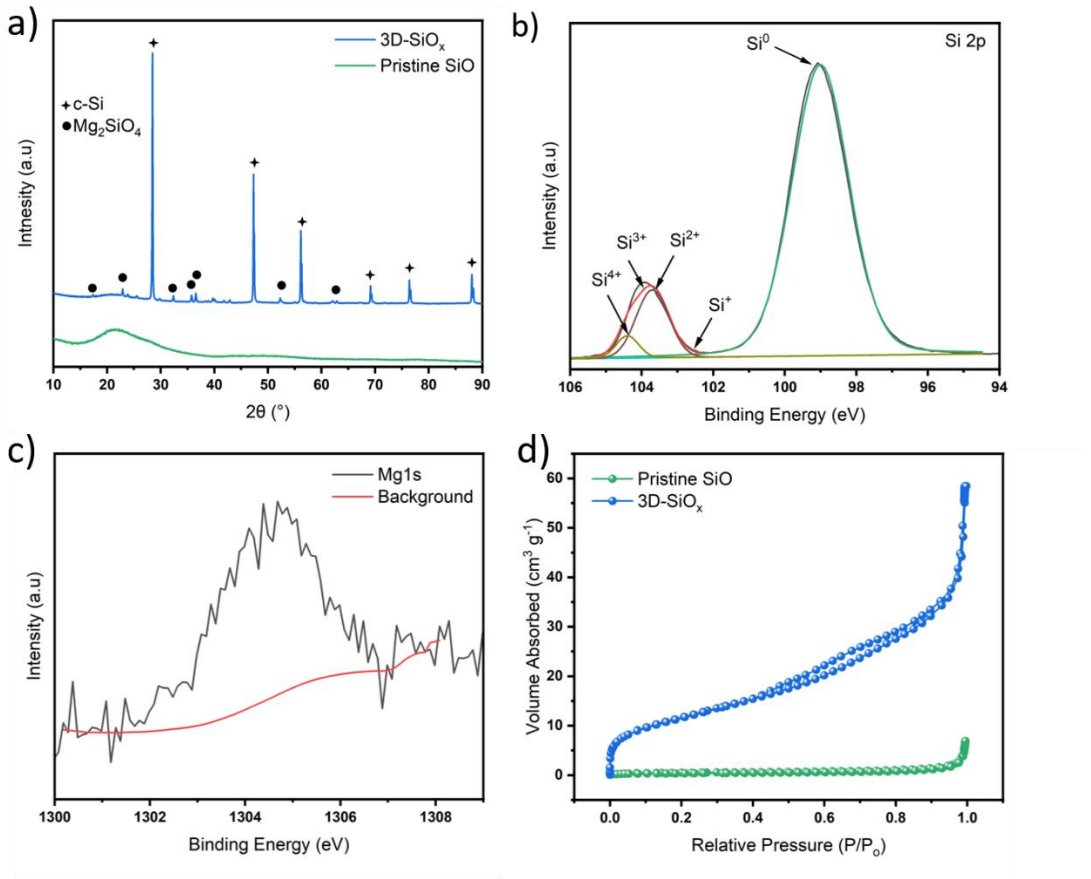

Figure 2: (a) XRD pattern for pristine SiO and 3D-Si/SiO_x, (b) Deconvoluted Si 2p spectrum of 3D-Si/SiO_x, (c) Mg1s spectra, and (d) N_2 isotherms.

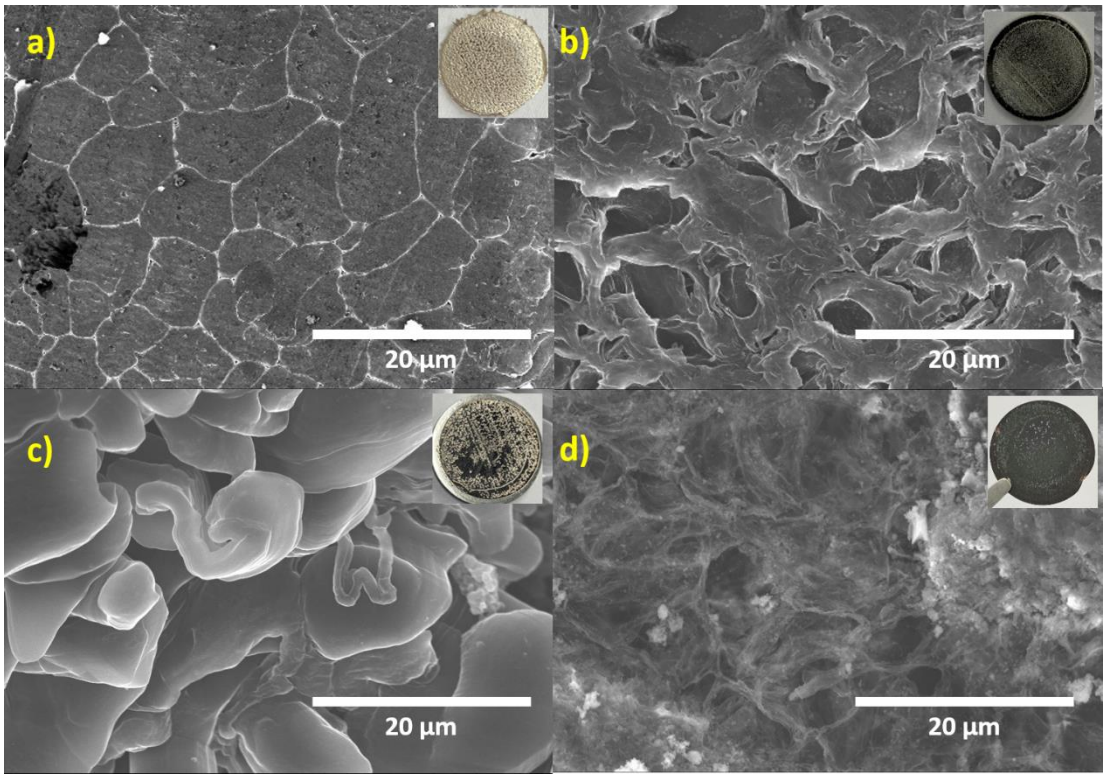

Figure 3: Surface SEM images of electrodes after lithium plating and stripping: (a, b) 3D-Si/SiO_x and (c, d) pristine SiO, respectively.

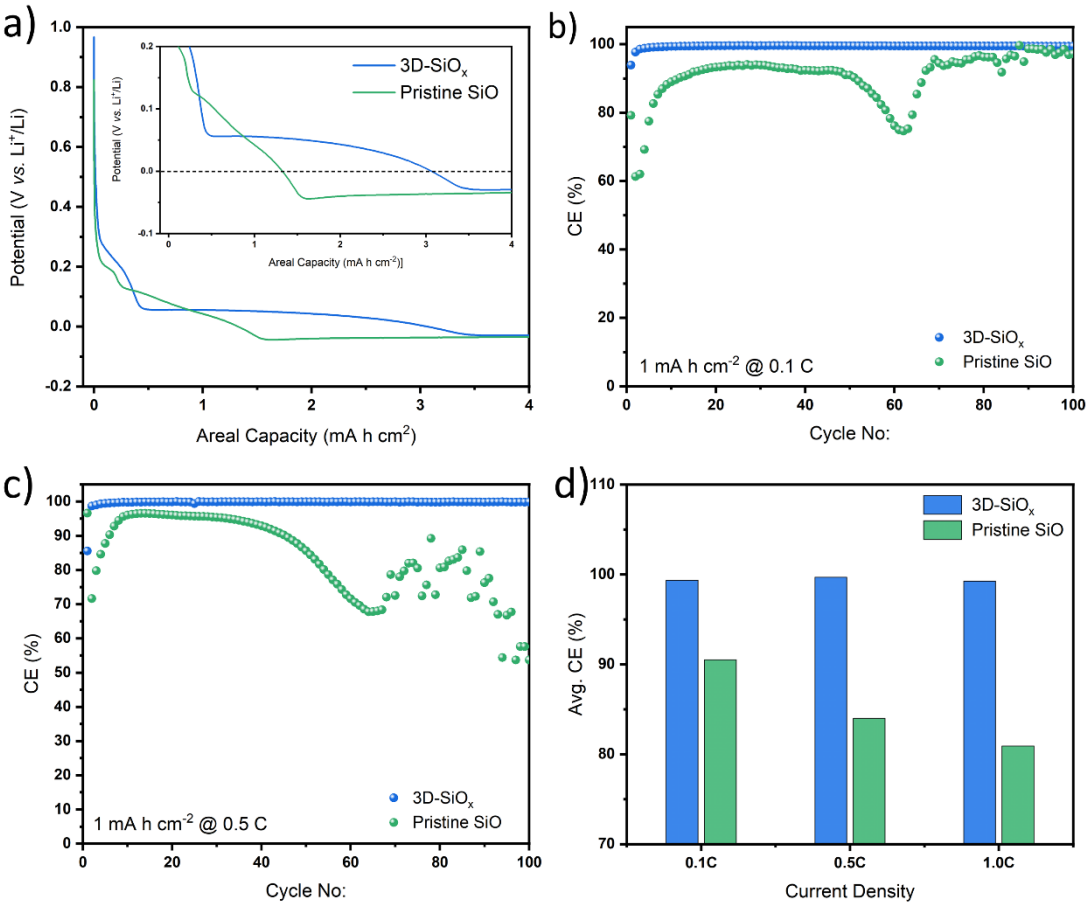

Figure 4: (a) Voltage profile at 0.1C, (b and c), cycle performance at 0.1, 0.5, and 1.0C, respectively, and (d) average coulombic efficiency of pristine SiO and 3D-Si/SiO_x

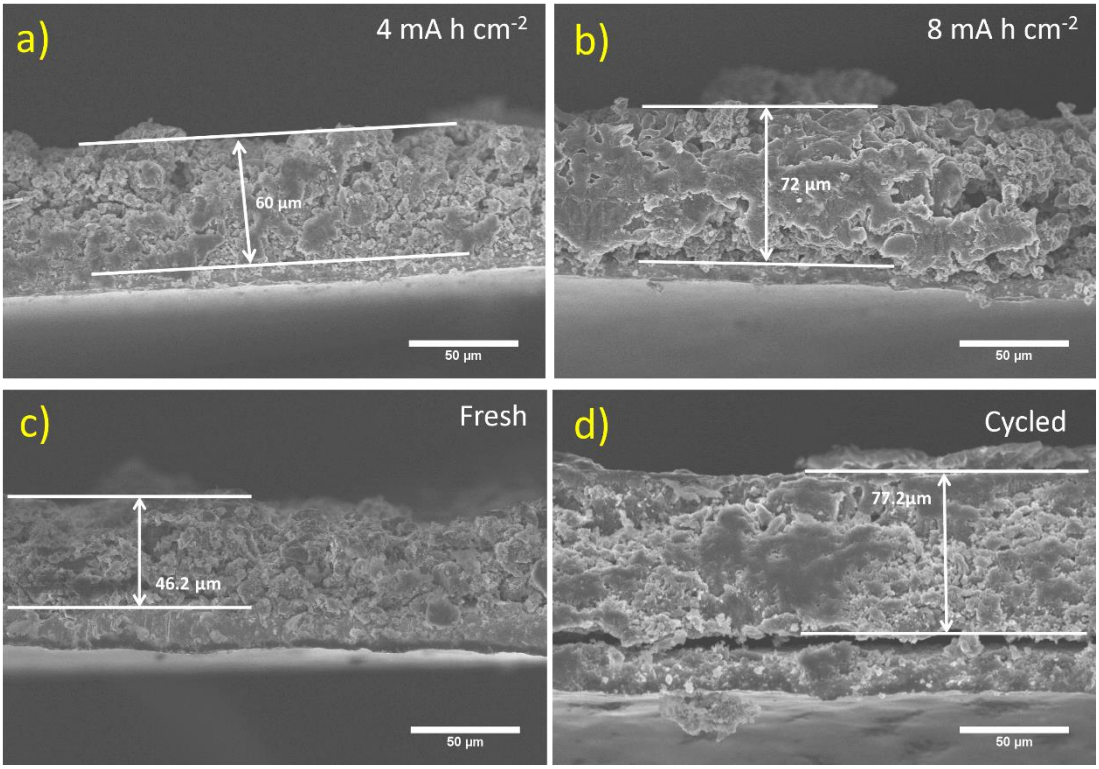

Figure 5: SEM Cross-section images of 3D-Si/SiO_x. (a) 4mAh cm^{-2} Li plating, (b) 8mAh cm^{-2} Li plating, (c) as-prepared, and (d) after 300^{th} cycle.

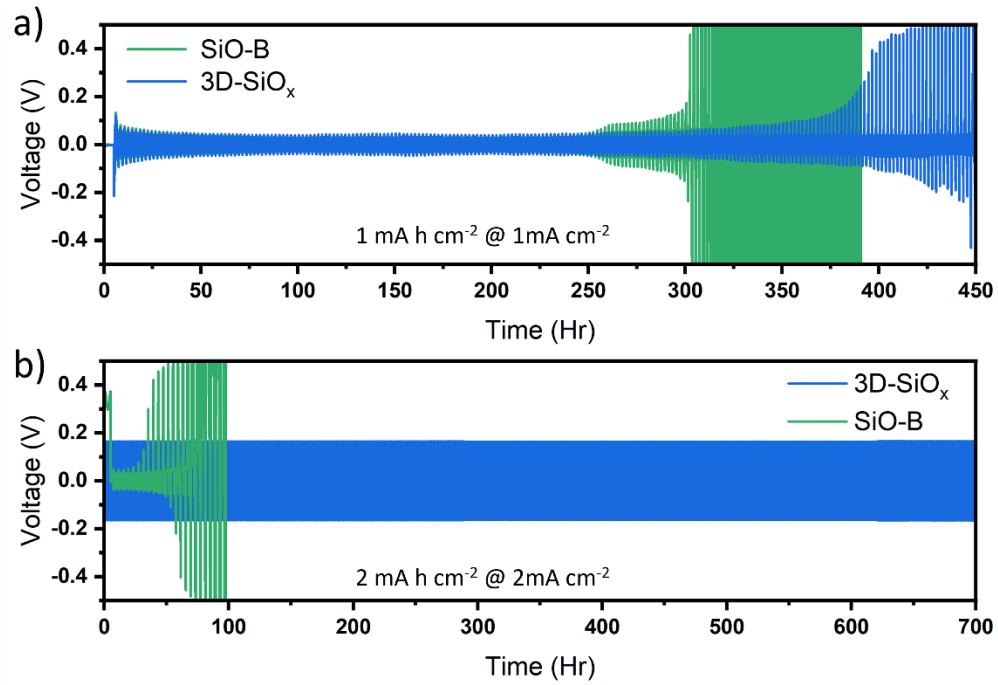

Figure 6: Symmetric cell data for Pristine SiO and 3D-Si/SiO_x at different utilization capacity

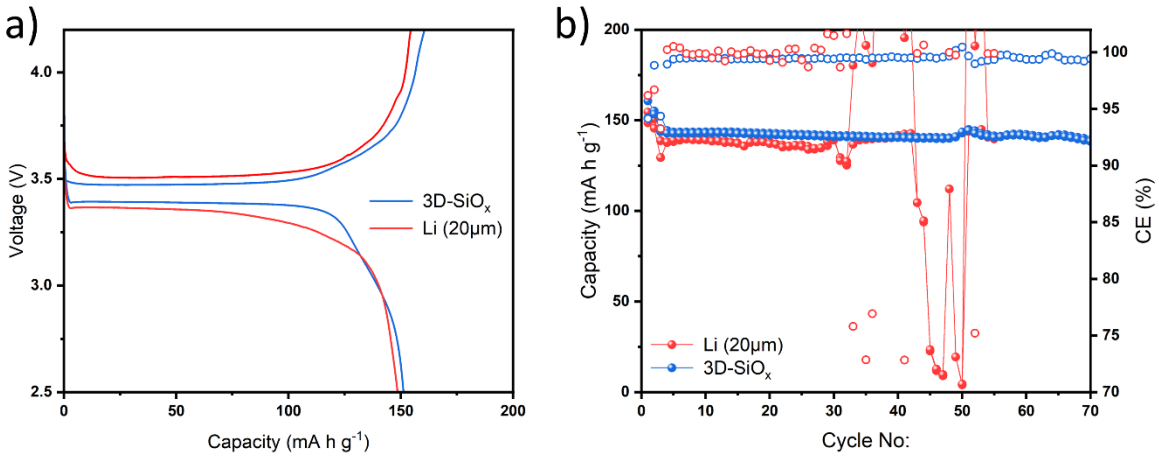

Figure 7: (a) Voltage profiles and (b) Cycle performances of the coin full cell using and LFP/3D-Si/SiO_x and of LFP/Li(20μm).

Table: 1. Summary of BET analysis for SiO and 3D-Si/SiO_x

Samples	Surface area (m^2 g^{-1})	Pore Volume (cm^3 g^{-1})	Pore Diameter (nm)
SiO	1.273	0.0065	7.35
3D-Si/SiO_x	42.35	0.078	20.41